

Experimental and numerical studies on the thermal analysis of the plate in indirectly fired continuous heat treatment furnace[†]

Young-Deuk Kim¹, Deok-Hong Kang² and Woo-Seung Kim^{3,*}

¹Department of Mechanical Engineering, Hanyang University, Seoul, 133-791, Korea

²Department of Energy Research, Research Institute of Industrial Science & Technology, Pohang, 790-600, Korea

³Department of Mechanical Engineering, Hanyang University, Ansan, 426-791, Korea

(Manuscript Received March 7, 2008; Revised August 29, 2008; Accepted September 3, 2008)

Abstract

Experimental and numerical studies were performed by considering convective and radiative heat transfer to predict the transient thermal behavior of a plate in an indirectly fired continuous heat treatment furnace. The temperature profiles in the plate were determined by solving the transient one-dimensional heat conduction equation in conjunction with appropriate boundary conditions by using a time marching scheme. The results obtained from the transient analysis were substantiated by comparing with experimental results. Additionally, parametric investigations were performed to examine how the thermal behavior of the plate is affected by plate and refractory emissivities, charging temperature and residence time of the plate, gas temperature of the work and drive sides of the heat treatment furnace, and plate thickness.

Keywords: Indirectly fired continuous heat treatment furnace; Thermal analysis; View factor; Optimization; Plate

1. Introduction

Indirectly fired heat treatment furnaces are widely used in metallurgy, paint enameling, the pharmaceutical industry, and other situations where it is necessary to control the furnace atmosphere. In most heat treatment processing of metals, scaling and decarburization may result in metal loss and lead to poor surface finishing [1]. Undesirable effects such as scaling and decarburization are strongly dependent on the residence time of the plate in the high temperature zones of the furnace and on the furnace atmosphere. Therefore, it is necessary to minimize or eliminate the undesirable effects of furnace gases. For this purpose, high temperature indirectly fired heat treatment furnaces, in which the products of combustion are separated from the me-

tal being heated, are used. The dominant mode of heat transfer in the indirectly fired heat treatment furnaces is the radiative heat transfer from the radiant tubes to the various surfaces of the furnace enclosure.

Rigorous thermal analysis of indirectly fired heat treatment furnaces is difficult due to the number of furnace attributes and processes that must be considered, including three-dimensional turbulent flow, heat transfer, chemical kinetics and thermodynamics in the radiant tubes, radiation and convection heat transfer in the furnace and inside the radiant tubes, and conduction heat transfer in the plate. A number of numerical and experimental studies have performed thermal analysis for a simplified mathematical model of a furnace [2-5].

The modeling of combustion in radiant tubes was comprehensively performed by Harder et al. [2] and Lisienko et al. [3]. Harder et al. [2] demonstrated that the longitudinal wall temperature variation for a straight through radiant tube is less than 50°C at a furnace operating temperature of 960°C.

[†] This paper was recommended for publication in revised form by Associate Editor Ohchae Kwon

* Corresponding author. Tel.: +82 31 400 5248, Fax.: +82 31 418 0153

E-mail address: wskim@hanyang.ac.kr

© KSME & Springer 2009

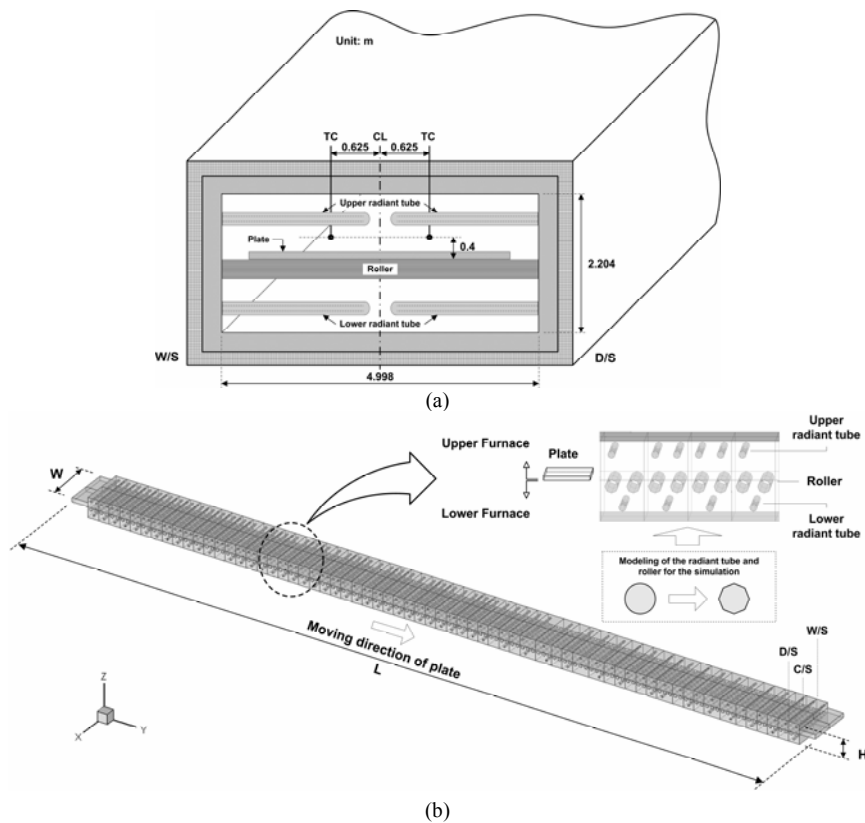


Fig. 1. (a) Physical model and (b) numerical modeling of the indirectly fired continuous heat treatment furnace.

Ramamurthy et al. [4] predicted the transient thermal behavior of the load and furnace walls and the furnace thermal efficiency for a batch reheating furnace. The heat flux at the radiant tube surface was specified and the lower furnace was not considered by assuming that the bottom surface of the load is adiabatic. The net radiation exchange between the load, the radiant tube surfaces, and the furnace walls was calculated by using the radiosity method, and the gases contained in the furnace were assumed to be radiatively nonparticipating. They performed extensive parametric investigations of the effects of load and refractory emissivities, load thermophysical properties and thickness as well as the effects of the fuel firing rate and cyclic furnace loading on the thermal performance. It was found that convective heat transfer to the load was negligible compared to the radiative transport.

Chapman et al. [5] developed a one-dimensional mathematical model to predict the steady state thermal performance of natural gas fired once-through and single-ended radiant tubes and a transient, zero-dimension-

nal (“stirred furnace”) model to predict the thermal performance and the temperature distribution in the load inside a batch directly fired furnace without considering the lower furnace. They showed that the typical temperature variation of the longitudinal wall of a blind-ended radiant tube is lower than about 25°C and 60°C at furnace operating temperatures of about 980°C and 870°C, respectively.

As mentioned above, most of the experimental and numerical studies have been performed for only simplified indirectly fired heat treatment furnace models. In the present study, experiments were conducted to predict the transient thermal behavior of the plate and gas in the furnace for the industrial heat treatment process of a plate. In addition, numerical analysis of radiative heat exchange in the furnace was also performed by solving the mathematical model simplified by several assumptions.

The furnace considered in this study consists of a total of 18 regions including 1 inlet region, 3 charging regions, 10 reheating regions, 3 discharging regions, and 1 outlet region. All of the regions are situated alo-

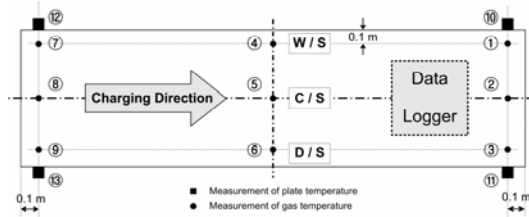


Fig. 2. Specification of the test plate for which temperature was measured.

ng the length of the furnace to reach the plate normalization temperature. The furnace is equipped with 172 blind-ended radiant tubes in the upper furnace and with 102 blind-ended radiant tubes and 135 rollers in the lower furnace. The radiant tubes in the furnace are irregularly set up along the length of the furnace. In the present study, numerical implementation of the one-dimensional transient thermal behavior of a plate was performed for the furnace shown in Fig. 1. To substantiate the validity of numerical results, the simulation results were compared with the experimental results. The gas temperatures in the furnace obtained from the experiment were used as the initial and boundary conditions for the numerical analysis. Also, parametric investigations were performed to examine how the thermal behavior of the plate is affected by plate and refractory emissivities, charging temperature and residence time of the plate, gas temperature of the work and drive sides of the heat treatment furnace, and plate thickness.

2. Experimental model

2.1 Experimental process

An experiment was conducted to substantiate the validity of the present numerical results and offer the initial and boundary conditions for the numerical analysis. A physical model of the furnace considered is depicted in Fig. 1(a). The blind-end radiant tube is used in the furnace to combine the advantages of a simple shape, uniform temperature distribution, and a high thermal efficiency. A typical configuration consists of two concentrically arranged tubes with the outer tube being closed at one end. Natural gas and air enter the inner tube via a recuperator burner and combust as they pass towards the closed end. At the closed end, the products of combustion turn 180° and return through the annular space separating the inner and outer tubes. Two blind-end radiant tubes were installed along the width of the furnace on both the W/S

Table 1. Base configuration parameters for the furnace and test plate.

Furnace dimensions	Length (m)	84.7
	Height (m)	2.204
	Width (m)	4.998
Material of plate		Alloy steel
Plate size ($H_p \times W_p \times L_p$) (m)		0.04 × 1.3 × 6.09
Residence time of plate (min)		79.45
Charging temperature of plate (°C)		37.24
Normalization temperature of plate (°C)		890
Time interval of data acquisition (sec)		10

Table 2. The position and usage of the thermocouple.

Number and position of thermocouple		Distance from bottom surface of the test plate (m)
①, ④, ⑦	W/S	0.02
②, ⑤, ⑧	C/S	0.02
③, ⑥, ⑨	D/S	0.02
⑩, ⑫	W/S	0
⑪, ⑬	D/S	0
Symbol		Usage
Square		Measurement of gas temperature
Circle		Measurement of plate temperature

and D/S sides.

As shown in Table 1, the furnace is 2.204 m in height, 4.998 m in width, and 84.7 m long. The test plate is 0.04 m thick and the charging temperature, normalization temperature, and residence time for the plate within the furnace was 39.2°C, 890°C, and 79.5 min, respectively. To protect the plate from oxidation and decarburization, the cold plate is continuously inserted into the center side of the furnace enclosure which is filled with fully heated inert gases such as argon or nitrogen. The thermocouples (Mineral insulated, Type K, 0.003 m diameter) are set up to measure the center plane temperature of the plate and gas temperature in the furnace, as shown in Fig. 2 and Table 2. Measured temperature data are stored in a data logger at ten-second intervals. The experimental setup and procedures are discussed in more detail in Kang et al. [6].

2.2 Experimental results

The temporal variations of the test plate (TC: ①-

Table 3. Time and distance required to reach the normalization temperature for each test plate position.

Number of thermocouple	Height (H_p) (m)	Position	880°C		890°C	
			Time (min)	Distance (m)	Time (min)	Distance (m)
①	0.02	W/S	46.45	32.952	51.78	37.343
②		C/S	46.62	33.049	52.45	37.676
③		D/S	43.95	31.462	48.62	34.453
④		W/S	58.12	40.491	71.28	56.541
⑤		C/S	58.78	40.821	68.95	54.198
⑥		D/S	50.28	36.114	62.95	43.712
⑦		W/S	59.95	41.403	74.62	68.866
⑧		C/S	58.78	40.281	69.62	54.859
⑨		D/S	48.95	34.789	66.78	49.990

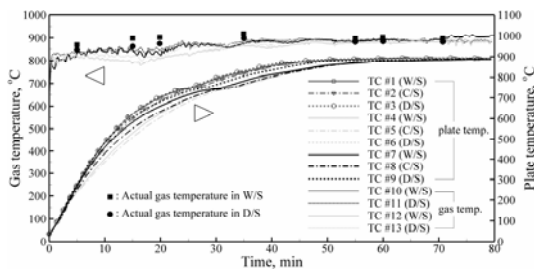


Fig. 3. Temporal variations of the plate and gas temperatures.

⑨) and gas (TC: ⑩–⑬) temperatures obtained from the experiment are shown in Fig. 3. About 88.7% of the radiant tubes operated normally due to fire extinguishing of about 31 radiant tubes at the W/S of the furnace during the industrial heat treatment process of the plate. Therefore, the gas temperature of the W/S is generally lower than that of the D/S, as shown in Fig. 3. Also, the variations of the gas temperatures at the W/S and D/S measured at the different positions (front and rear sections) of the plate are similar. Table 3 shows the time and distance required for each plate position to reach the normalization temperature.

It takes about 60 minutes for all positions of the plate to attain a temperature within plus or minus 10°C of the normalization temperature. Up to a residence time of about 50 minutes for the plate within the furnace, the rate of the plate temperature increase at the W/S and D/S, where the plate receives more energy from the bottom, top, and side of the plate, is higher than that of the plate at the center of the furnace. However, the temperature deviation of the plate at the W/S, C/S, and D/S of the furnace becomes uniform within 5°C after 50, 65, and 60 minutes for the three positions (front, middle, and rear sections) of the plate, respectively. Also, when the residence time of the plate is about 14.78 min ($L=11.883$ m), the

maximum temperature deviation for all positions of the plate is rather large at about 115°C, but the plate temperatures become uniform with a maximum temperature deviation of 5°C at the outlet region of the furnace.

3. Numerical model

3.1 Governing equations and boundary conditions

For analysis of radiative heat exchange in the furnace, the entire surface of the furnace enclosure is divided into a finite number of zones, as shown in Fig. 1. The outer surface temperature of the radiant tube is assumed to be constant and a simplified mathematical model is used, which does not consider detailed processes occurring in the radiant tube.

The main assumptions and features of the model used in this study are as follows:

(i) The longitudinal temperature profile of the outer surface of the radiant tube is uniform. This assumption is reasonable because the typical temperature variation of the longitudinal wall of a straight through radiant tube is less than about 50°C at a furnace operating temperature of about 960°C and that of a blind-ended radiant tube is also less than about 25°C and 60°C at a furnace operating temperature of about 980°C and 870°C, respectively [2, 5].

(ii) The furnace enclosure was divided into 130 gas zones (upper furnace: 66 and lower furnace: 64) and the temperature was uniform within each zone.

(iii) All surfaces of the furnace are diffuse emitters and diffuse reflectors, and the radiative properties are uniform and independent of surface direction.

(iv) The temperature at the surface of each zone is uniform.

(v) The wall temperature of each zone is equal to the gas temperature at the same position of the furnace.

(vi) The outer surfaces of the furnace are assumed to be adiabatic.

(vii) Conductive heat transfer between the roller and the plate is neglected due to short contact time.

(viii) The gases in the furnace are radiative nonparticipating, because the furnace is usually filled with inert gases such as argon or nitrogen.

(ix) The plate is continuously inserted into the center side of the furnace, and the radiative heat exchange between the lower and upper portions of the furnace is neglected.

To predict the temperature distribution of the plate,

the following one-dimensional transient conduction equation is considered:

$$\rho c \frac{\partial T_p}{\partial t} = \frac{\partial}{\partial z} \left(k \frac{\partial T_p}{\partial z} \right) \quad (1)$$

where ρ , c , k , t , and T_p represent the density, specific heat, conductivity, time, and plate temperature, respectively. The conduction in the x- and y-direction of the plate can be neglected in comparison to advection due to the large length-to-thickness ratio and large value of the Peclet number ($Pe = \rho c V_p L_p / k$).

The boundary condition for the top and bottom surfaces of the plate exposed to the heat flux from the radiant tubes and the furnace walls is

$$-k \frac{\partial T_p}{\partial z} = -q_t \text{ or } q_t \quad (2)$$

where q_t is the total heat flux (radiative and convective), which is expressed as:

$$q_t = q_{rad} + q_{conv} \quad (3)$$

To calculate the radiative heat flux of Eq. (3), the following mathematical model is used [7, 8]:

$$q_{rad} = \frac{\sigma \epsilon_p}{1 - (1 - \epsilon_p)(1 - A_{gp})} (\epsilon_g T_g^4 - A_{gp} T_p^4) + \sigma \sum_{i=1}^{M \text{ or } N} \epsilon_{pw,i} (T_{w,i}^4 - T_p^4) \quad (4)$$

where the subscripts g , p , w , and i denote gas, plate, wall, and zone number, respectively, and the respective values of M and N represent the total number of surface zones in the lower and upper furnace.

The first term in the right hand side of Eq. (4) represents heat flux from the gases (CO₂, H₂O, and SO₂) to the plate surface and A_{gp} is the gas absorptivity. The first term of Eq. (4) is neglected in the present study because the argon or nitrogen gases in the furnace are radiative nonparticipating media. The second term represents heat flux from the wall to the plate surface. ϵ_{pw} , which is the direct-exchange factor between the walls and the plate, is modeled as [8, 9]:

$$\epsilon_{pw} = \epsilon_p \epsilon_w \tau_{gm} F_{pw} + \Delta \epsilon_{pw} \quad (5)$$

in which $\Delta \epsilon_{pw}$ is a correction factor for flame radiation

Table 4. Number of zones by furnace location.

	Location	Zone number	Total zone number
Lower furnace	Side wall	128	3,240
	Bottom wall	136	
	Roller	2,160	
	Radiant tube	816	
Upper furnace	Side wall	132	1,648
	Top wall	140	
	Radiant tube	1,376	

and becomes zero for the indirectly fired heat treatment furnace unlike in the directly fired reheating furnace in which the combustion of gases occurs directly in the furnace. The mean gas transmissivity for radiation from the plate and walls is calculated from

$$\tau_{gm} = 1 - A_{gm} \quad (6)$$

in which

$$A_{gm} = \frac{1}{2} (A_{gp} + A_{gw}) \quad (7)$$

A_{gm} is the mean gas absorptivity for radiation from the plate and walls. For a furnace filled with inert gases such as argon or nitrogen, the mean gas absorptivity is zero. The F_{pw} in Eq. (5) is the view factor between the plate and the wall. View factors are evaluated separately for the radiation coming from the upper and the lower parts of the furnace.

Given the above, Eq. (4) can be rearranged as:

$$q_{rad} = \sigma \epsilon_p \sum_{i=1}^{M \text{ or } N} \epsilon_{w,i} F_{pw,i} (T_{w,i}^4 - T_p^4) \quad (8)$$

Also, the convective heat flux in Eq. (3) is obtained as follows:

$$q_{conv} = h(T_{g,i} - T_p) \quad (9)$$

where h is the convective heat transfer coefficient.

3.2 View factor

A physical model of an indirectly fired heat treatment furnace with the dimensions and parameters presented in Tables 1 and 5, respectively, is shown in Fig. 1. To aid in the analysis of radiative heat ex-

change in the enclosure (furnace), the furnace with 18 regions is subdivided into 2 major zones (upper and lower) along the height of the furnace by the traffic line of the plate, 2 major zones (W/S and D/S) along the width of the furnace, and 66 (upper furnace) and 64 (lower furnace) major zones along the length of the furnace, as shown in Fig. 1. Additionally, the roller and radiant tube are subdivided into 16 surface zones for the radial and axial direction of the roller and radiant tube, respectively. Therefore, the upper and lower furnaces are divided into 1,648 and 3,240 surface zones, respectively. For the top and bottom surface of the plate, view factors evaluated separately for the 1,648 and 3,240 surface zones are obtained by zoning of the furnace enclosure and numerically calculating them along the length of the furnace with 0.12 m intervals. The number of zones by enclosure location is presented in Table 4.

The radiative view factor between two surfaces can be formulated as follows:

Table 5. Physical properties used in the model [4, 5]

Alloy steel:	
ρc (J/m ³ K)	k (W/mK)
2,816,000+768(T_p -600)	126-0.02105(T_p -600)
· Emissivity (ϵ_p)	: 0.5
· Thickness (H_p)	: 0.04 m
Miscellaneous:	
· Number of radiant tubes	
- Upper furnace	: 172
- Lower furnace	: 102
· Number of rollers	: 135
· Wall emissivity (ϵ_w)	: 0.9
· Heat transfer coefficient	: 1 W/m ² K
· Surface temperature of radiant tube	: 900°C
· Radius of radiant tube	: 0.101 m
· Radius of roller	: 0.180 m

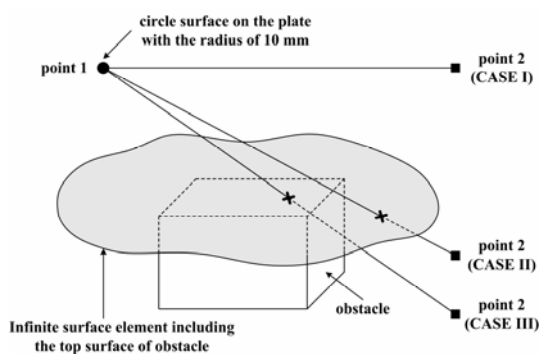


Fig. 4. Three cases of obstacle detection.

$$F_{A_i-A_j} = \frac{1}{A_i} \int_{A_i} \int_{A_j} \frac{\cos \theta_i \cos \theta_j}{\pi S^2} dA_j dA_i \quad (10)$$

where A_i and A_j are the surface area of the plate and wall, respectively. θ_i and θ_j are the angles between the surface normal and the line connecting dA_i and dA_j , respectively. S is the distance of the element surfaces dA_i and dA_j .

Many previous studies [10-13] have reported exact solutions of view factors for specific geometries, but it is difficult to find the exact solution for a general geometry. Specifically, when there are obstacles between two surfaces, as in this work, it is difficult to obtain exact solutions of view factors. Hence, for the purpose of obtaining the view factor for a general geometry, each surface is divided into finite elements, and then view factors can be calculated numerically by the definition given by Eq. (10). When there is an obstacle between two surfaces, an obstacle detection method can be used to find the view factor. Fig. 4 presents the three cases that can occur in detecting an obstacle.

The process of detecting the obstacle between point 1 on surface A_i and point 2 on surface A_j is as follows:

- (i) Calculate the direction vector between two points.
- (ii) Use the direction vector to construct the straight line through point 1.
- (iii) It is assumed that each surface of the obstacle is an infinite surface element and it is determined whether the straight line calculated by step 2 crosses this infinite surface element.
- (iv) If the straight line does not cross the infinite surface element (CASE I), then no obstacle exists between point 1 and point 2. However, if the straight line crosses the infinite surface element (CASE II and III), an intersection point is calculated.
- (v) When the calculated intersection point exists on

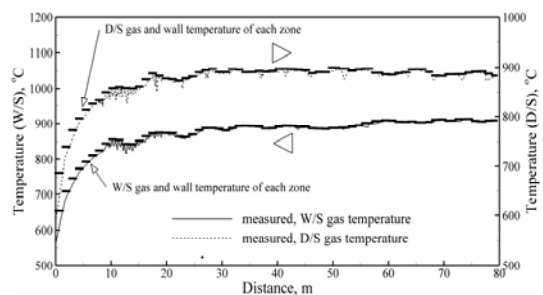


Fig. 5. Variation of the gas and wall temperatures along the axial direction.

the real finite surface of the obstacle (CASE III), then the obstacle exists between point 1 and point 2 and the integrand of Eq. (10) should be set equal to zero.

With the calculation process mentioned above, the view factors are calculated based on the thickness of the plate and x-directional position (W/S, C/S, and D/S) of the furnace. The sum total of the view factors from any surface zone should ideally be equal to 1. Using this model, the maximum percent error in the sum total of view factors for the specified furnace geometry was estimated to be less than 1%.

3.3 Analysis and validation

The governing Eq. (1) discretized with the finite volume method [14] is solved in conjunction with the boundary conditions given by Eqs. (8) and (9) by using a time marching scheme. The values of the alloy steel properties, other parameters, and furnace geometry used in the present study are given in Table 5. The variations of the gas and wall temperatures along the length of the furnace are shown in Fig. 5. The measured gas temperatures of the W/S and D/S represented in Fig. 5 are obtained by averaging the gas temperatures of the W/S and D/S measured at the different positions (front and rear sections) of the plate.

For the numerical implementation, the surface temperature of each zone is assumed to be equal to the gas temperature in the furnace and the gas temperatures of W/S and D/S in the furnace are assumed to be the maximum gas temperature at each gas zone, as obtained from experimental data. The convergence criterion used for iterations within an unsteady state is, $|T_p^{n+1} - T_p^n| / |T_p^{n+1}| \leq 10^{-5}$, where T_p is the plate temperature and n is the iteration level.

Comparisons of the center plane temperatures at W/S, C/S, and D/S obtained from the experiment and numerical simulation are illustrated in Fig. 6. Except for the inlet and some charging regions of the furnace,

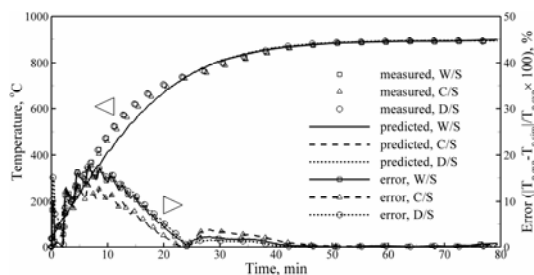


Fig. 6. Comparison of the present results (line) with those of experiment (symbol).

the present numerical results agree well with experimental data.

4. Results and discussion

The temporal variations of the center plane temperature of the plate have been numerically estimated for varying plate and refractory emissivities, charging temperature and residence time of the plate, gas temperature of the work and drive sides of a heat treatment furnace, and plate thickness.

4.1 Effect of plate and wall emissivities

Wall emissivities are assumed to be equal to 0.9 by a reasonable first approximation since emissivities are within a range of $0.85 \leq \epsilon_w \leq 0.93$ for inner walls of the furnace and outer walls of the radiant tube and roller at elevated temperatures. And the emissivity of alloy steel plate used in the experiment is assumed to be 0.5. To examine the effect of the plate emissivity on the heating pattern of the plate during the heat treatment process, simulations were performed by varying the plate emissivity, ϵ_p , from 0.1 to 0.8 while the other parameters were maintained at the values given in Tables 1 and 5. Fig. 7 depicts the variation of the plate center plane temperature with residence time

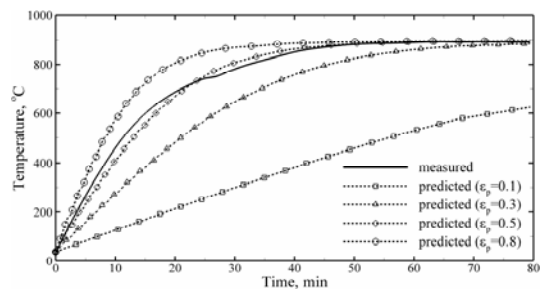


Fig. 7. Center plane temperature of the plate for varying plate emissivity.

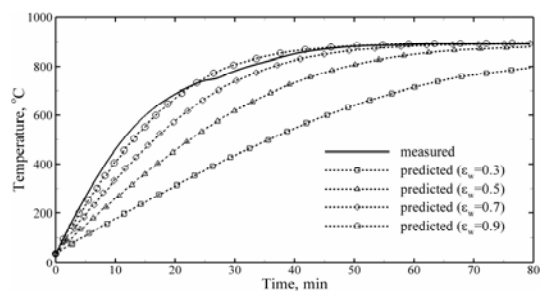


Fig. 8. Center plane temperature of the plate for varying wall emissivity.

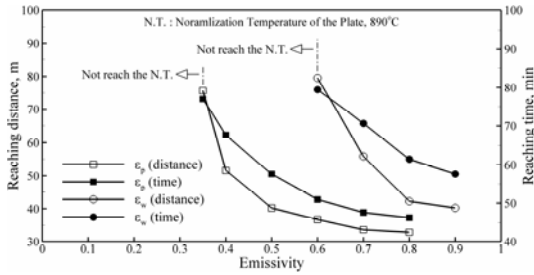


Fig. 9. Distance and time required to reach the normalization temperature of the plate for various emissivities of the plate and wall.

for different plate emissivities. As the emissivity of the plate increases, the plate temperature increases rapidly because the adsorption of radiant energy at the plate surface is higher at higher values of ϵ_p . For plate emissivities of 0.3 and 0.8, the plate temperature increases to the normalization temperature of the plate, within the maximum temperature deviation of 5°C, as the outlet region of the furnace is approached. However, the exit plate temperature with a plate emissivity of 0.1 is about 265°C lower than the normalization temperature of the plate.

With the residence time for the plate within the furnace, Fig. 8 depicts the center plane temperature of the plate with the wall emissivity, ϵ_w , varying from 0.3 to 0.9. For a wall emissivity of 0.7, the plate temperature increases to the normalization temperature of the plate, within a maximum temperature deviation of 4°C, near to the outlet region of the furnace. However, the exit plate temperatures with wall emissivities of 0.3 and 0.5 are about 96°C and 10°C, respectively, lower than the normalization temperature of the plate.

The distance and time required to reach the normalization temperature of the plate for various plate emissivities are presented in Fig. 9. For plate emissivities of 0.35 and 0.8, the time and distance increase about 34% and 88% and decrease about 20% and 18%, respectively, as compared to those of a plate emissivity of 0.5, which is similar to the experimental conditions. For a wall emissivity of 0.6, the time and distance needed to achieve the normalization temperature increase by about 38% and 98%, as compared to the time and distance obtained by using a wall emissivity of 0.9, which is similar to the experimental condition.

4.2 Effect of charging temperature

Fig. 10 shows the center plane temperature varia-

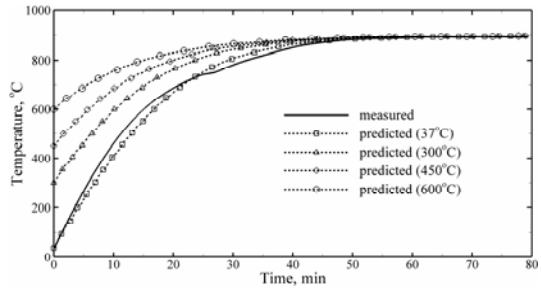


Fig. 10. Center plane temperature of the plate for various charging temperatures.

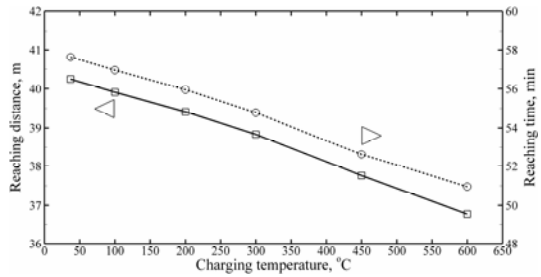


Fig. 11. Distance and time required to reach the normalization temperature of the plate for various charging temperatures of the plate.

tion with residence time for various charging temperatures. The increase rate of the plate temperature is shown to be small relative to variations in the charging temperature of the plate.

As the charging temperature of the plate increases from 37°C to 100°C, 300°C, and 600°C, the residence time for the plate within the furnace slightly decreases by about 1%, 5%, and 12% and the distance decreases by about 1%, 4%, and 9%, respectively, as shown in Fig. 11. The reduced residence times indicate a higher production rate of the furnace for the same normalization temperature of the plate. However, the charging temperature of the plate does not significantly affect the production rate of the furnace.

4.3 Effect of residence time

Fig. 12 shows the center plane temperature of the plate for various residence times. The center plane temperature reaches the normalization temperature of the plate for all residence times except at about 40 min ($V_p \approx 0.035$ m/sec). The exit plate temperature for the residence time of about 40 min is about 21°C lower than the normalization temperature of the plate.

The distance and time required to reach the normalization temperature of the plate for various resi-

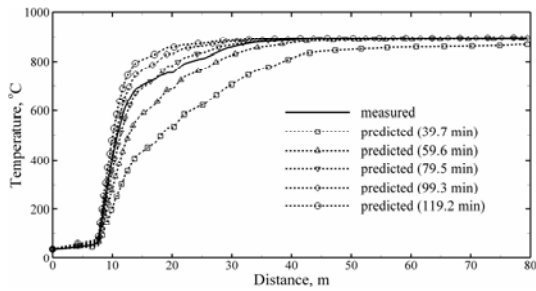


Fig. 12. Center plane temperature of the plate for various residence times.

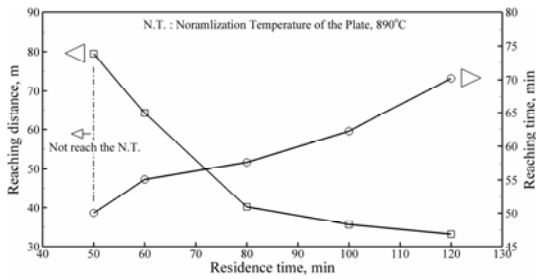


Fig. 13. Distance and time required to reach the normalization temperature of the plate for various residence times of the plate.

dence times for the plate within the furnace are shown in Fig. 13. As the residence time increases from about 50 min ($V_p \approx 0.028$ m/sec) to about 60 min ($V_p \approx 0.024$ m/sec), 80 min ($V_p \approx 0.018$ m/sec), 100 min ($V_p \approx 0.014$ m/sec), and 120 min ($V_p \approx 0.012$ m/sec), the time required to reach the normalization temperature of the plate gradually increases by about 10%, 15%, 24%, and 40%, respectively. However, the distance greatly decreases by about 19%, 49%, and 55% up to the residence time of 100 min, after which the decrease rate becomes negligible, as shown in Fig. 13. These results indicate that the minimum distance required to reach the normalization temperature of the plate is about 30 m irrespective of the residence time for the plate within the furnace.

Although increasing residence time significantly affects plate temperature uniformity, doing so also reduces the plate production rate. Hence, the residence time and, thus, the plate velocity needs to be optimized in order to achieve a balance between production rate, furnace length, and exit plate temperature, as shown in Fig. 13.

4.4 Effect of gas temperature difference between W/S and D/S

It is possible for the radiant tubes at the W/S and

Table 6. Exit temperature and maximum temperature deviation of the plate for various cases.

Case	ΔT^a (°C)	Exit plate temperature (center) (°C)	$T_{p,d}^b$ (°C)
Experimental result	0	892	2.42
Numerical result	0	896	3.19
1	15	904	14.97
2	30	912	26.71
3	45	920	38.40
4	50	923	42.29
5	100	951	80.97

- a: W/S experimental gas temperature + ΔT
- b: Maximum temperature deviation

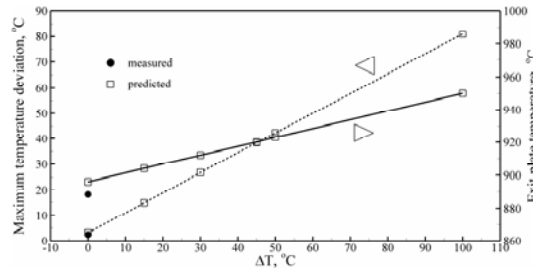


Fig. 14. Effect of the W/S and D/S gas temperature difference on the maximum temperature deviation and exit temperature of the plate.

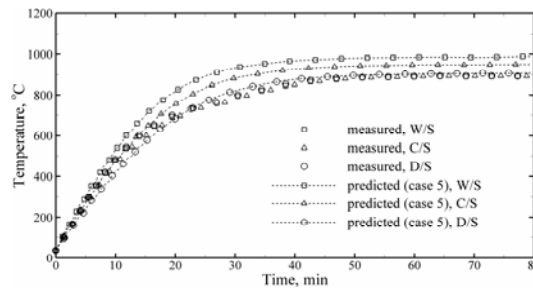


Fig. 15. Measured and predicted (case 5) center plane temperature of the plate.

D/S to work under different operating conditions caused by unexpected circumstances such as fire extinguishing in the radiant tube during the industrial heat treatment process of the plate.

Table 6 and Fig. 14 show the maximum temperature deviation and exit temperature of the plate under various gas temperature differences in the W/S and D/S. Fig. 15 shows the center plane temperature of the plate in the W/S, C/S, and D/S of the furnace for case 5. As the gas temperature of the W/S increases relative to that of the D/S, the maximum temperature deviation and exit temperature of the plate increase almost linearly. Thus, the difference between the W/S and D/S gas temperatures significantly affects tem-

perature uniformity and the exit temperature of the plate.

4.5 Effect of plate thickness

In general, a plate of length in the range of $6 \text{ m} \leq L_p \leq 20 \text{ m}$ and thickness in the range of $0.0045 \text{ m} \leq H_p \leq 0.05 \text{ m}$ is used in the heat treatment processing. Fig. 16 shows the center plane temperature of the plate for various plate thicknesses. The heating capacity of the plate is shown to be excellent as the plate thickness becomes thin. As the plate thickness decreases from 0.04 m to 0.03 m, 0.02 m, and 0.01 m, the time and distance required to reach the normalization temperature of the plate decrease by about 16% and 15%, about 22% and 21%, and about 34% and 31%, respectively. However, as the plate thickness increases from 0.04 m to 0.05 m, the time and distance increase by about 18% and 30%.

The distance and time required to reach the normalization temperature of the plate for various plate residence times and thicknesses are shown in Fig. 17. To maximize the production rate of the plate, it is required that the residence time for the plate within the furnace be reduced. Therefore, to maximize the production rate of the plate as the plate thickness in-

creases from 0.01 m to 0.02 m, 0.03 m, 0.04 m, and 0.05 m, the residence time of the plate should be maintained at a maximum of 15 min ($V_p \approx 0.094 \text{ m/sec}$), 30 min ($V_p \approx 0.047 \text{ m/sec}$), 40 min ($V_p \approx 0.035 \text{ m/sec}$), 55 min ($V_p \approx 0.026 \text{ m/sec}$), and 70 min ($V_p \approx 0.02 \text{ m/sec}$), respectively.

5. Conclusions

From the transient thermal analysis of the plate in the heat treatment furnace, the following conclusions can be made:

- As the plate and wall emissivities increase, the time and distance required to reach the normalization temperature of the plate decrease, and to obtain the plate normalization temperature, the plate and wall emissivities must be above about 0.35 and 0.6, respectively.
- The rate of change of the time and distance required to reach the plate normalization temperature is quite small relative to the increasing rate of the charging temperature. However, the effect of the charging temperature on the plate is negligible relative to the effects of varying the other parameters considered in this study.
- Although an increase in residence time significantly affects the uniformity of the plate temperature, it reduces the plate production rate. Also, the residence time of the plate needs to be above about 50 min for the plate normalization temperature to be reached.
- The gas temperature difference between the W/S and D/S greatly affects the temperature uniformity and exit temperature of the plate. Thus, the heat treatment process must be maintained below a W/S and D/S gas temperature difference of about 15°C to attain the plate with suitable temperature uniformity and a normalization temperature within plus or minus 10°C .
- To maximize the production rate of the plate as the plate thickness increases from 0.01 m to 0.02 m, 0.03 m, 0.04 m, and 0.05 m, maximum plate residence times of 15 min ($V_p \approx 0.094 \text{ m/sec}$), 30 min ($V_p \approx 0.047 \text{ m/sec}$), 40 min ($V_p \approx 0.035 \text{ m/sec}$), 55 min ($V_p \approx 0.026 \text{ m/sec}$), and 70 min ($V_p \approx 0.02 \text{ m/sec}$), respectively, should be maintained.

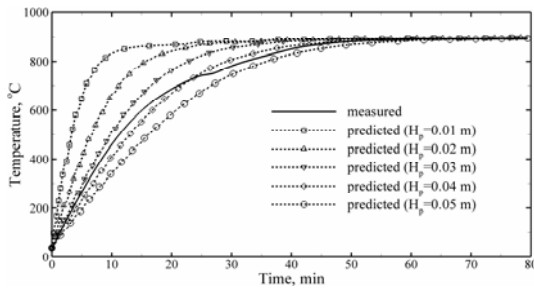


Fig. 16. Center plane temperature of the plate for various plate thicknesses.

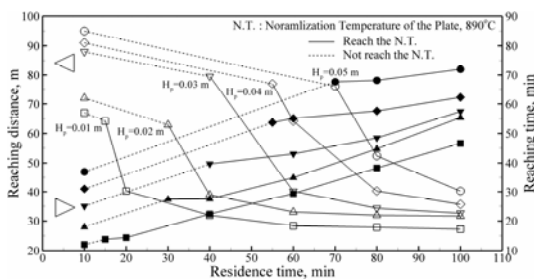


Fig. 17. Time and distance required to reach the normalization temperature of the plate for various plate thicknesses and velocities.

Nomenclature

A	: Surface area
A_{gm}	: Mean gas absorptivity for radiation from plate and walls
A_{gp}	: Gas absorptivity for radiation from the plate
A_{gw}	: Gas absorptivity for radiation from the walls
c	: Specific heat
C/S	: Center side of the furnace
D/S	: Drive side of the furnace
F_{pw}	: View factor between plate and wall
H	: Furnace height
h	: Convective heat transfer coefficient
H_p	: Plate thickness
k	: Thermal conductivity
L	: Furnace length
L_p	: Plate length
M	: Total number of surface zones in the lower furnace
N	: Total number of surface zones in the upper furnace
q	: Heat flux
S	: Distance of element surfaces dA_i and dA_j
T	: Temperature
t	: Time
TC	: Thermocouple number
V_p	: Plate velocity
W	: Furnace width
W_p	: Plate width
W/S	: Work side of the furnace
x, y, z	: Cartesian coordinates

Greek Symbols

$\Delta\epsilon_{pw}$: Correction factor for flame radiation
ϵ	: Emissivity
ϵ_{pw}	: Direct-exchange factor between plate and walls
θ_i, θ_j	: Angle between the surface normal and the line connecting dA_i and dA_j
ρ	: Density
σ	: Stefan-Boltzmann constant
τ_{gm}	: Mean gas transmissivity between plate and walls

Subscripts

$conv$: Convection
d	: Deviation
g	: Gas
i, j	: Zone index number

p	: Plate
rad	: Radiation
t	: Total
w	: Wall

References

- [1] R. Pritchard, J. J. Guy and N. E. Connor, *Handbook of industrial gas utilization*, Van Nostrand Reinhold Company, New York, USA, (1977).
- [2] D. C. Harder, R. Viskanta and S. Ramadhyani, Evaluation and modeling of gas-fired radiant tubes, *Proc. of ASME Nat. Heat Trans. Conf.*, 1 (1988) 67-77.
- [3] V. G. Lisienko, F. R. Skylar, Y. V. Dryuchenkov, L. N. Toritsyn, V. V. Vokov and A. I. Tikhostiskii, Combined solution of the problem of external heat transfer and heat transfer inside a gas radiation tube for thermal furnaces with a protective atmosphere, *J. Eng. Phys.*, 50 (1) (1986) 70-76.
- [4] H. Ramamurthy, S. Ramadhyani and R. Viskanta, Modeling of heat transfer in indirectly-fired batch reheating furnace, *Proc. of the ASME/JSME Therm. Eng. Conf.*, 5 (1991) 205-215.
- [5] K. Chapman, R. F. Harder, S. Ramadhyani and R. Viskanta, Radiative heat transfer, *Annual Report January 1987 - March 1988*, Purdue Univ., USA, (1988).
- [6] D. H. Kang, D. S. Kwag, W. S. Kim and Y. K. Lee, A study on the estimation of one-dimensional heat fluxes on the slab in reheating furnace by using inverse analysis, *Trans. of the KSME Part B*, 27 (1) (2003) 61-68.
- [7] D. Lindholm and B. Leden, A finite element method for solution of the three-dimensional time-dependent heat-conduction equation with application for heating of steels in reheating furnaces, *Num. Heat Trans. Part A*, 35 (1999) 155-172.
- [8] B. Leden, Mathematical reheating furnace models in STEELTEMP, *Proc. of Int. Conf. SCANHEATING*, MEFOS, Lueta, Sweden, 2 (1985).
- [9] B. Leden, STEELTEMP – a program for temperature analysis in steel plants, *Scand. J. Metall.*, 15 (1986) 215-223.
- [10] M. F. Modest, *Radiation heat transfer*, McGraw-Hill, New York, USA, (1993).
- [11] R. Siegel and J. R. Howell, *Thermal radiation heat transfer*, McGraw-Hill, New York, USA, (1982).
- [12] J. R. Howell, *Radiation configuration factor*, McGraw-Hill, New York, USA, (1982).
- [13] E. M. Sparrow and R. D. Cess, *Radiation heat tra-*

nsfer, McGraw-Hill, New York, USA, (1976).

- [14] S. V. Patankar, *Numerical heat transfer and heat flow*, Hemisphere Publishing Corp., Washington D. C., USA, (1980).



Young-Deuk Kim is a graduate student at Hanyang University in Seoul, Korea. He earned his B.S. in Mechanical Engineering from Korea Maritime University in 2002 and his M.S. in mechanical engineering from Hanyang university in 2004. His current research areas are modeling of automotive aftertreatment catalysts, optimal design of thermal systems, and phase change modeling with free surface flow.



Deok-Hong Kang is a senior researcher at the RIST (Research Institute of Industrial Science and Technology) in Pohang, Korea. He earned his B.S. and M.S. in mechanical engineering from Hanyang University in 1989 and 1993, respectively, and his Ph.D. in mechanical engineering from POSTECH in 2004. His current research areas are mathematical modeling for combustion control, furnace optimization control system, and energy saving engineering in all kinds of furnaces.



Woo-Seung Kim is a professor in mechanical engineering at Hanyang University in Ansan, Korea. He earned his B.S. in Mechanical Engineering in 1981 from Hanyang University and his M.S. and Ph.D. in mechanical engineering from North

Carolina State University in 1986 and 1989, respectively. His current research areas are modeling of automotive aftertreatment systems, inverse heat transfer problems, optimal design of thermal systems, and phase change heat transfer problems with free surface flow.